

A Low-Noise High-Density Alkalimetal Scalar Magnetometer

S. J. Smullin, I. M. Savukov, G. Vasilakis, R. K. Ghosh, and M. V. Romalis

Physics Department, Princeton University, Princeton, NJ 08542, USA

(Dated: February 13, 2019)

We present a theoretical and experimental study of an atomic magnetometer operating in geomagnetic field range based on oscillating field-driven Zeeman resonance in a high-density optically-pumped potassium vapor. We show that the fundamental field sensitivity is determined by the rate of spin-exchange collisions even though the resonance linewidth width can be made much smaller than the spin-exchange rate by pumping most atoms into a stretched spin state. We also describe an experimental implementation of a high-density atomic gradiometer with a noise level below $10 \text{ fT Hz}^{-1/2}$, fractional field sensitivity below $10^{-9} \text{ Hz}^{-1/2}$, and an active measurement volume of about 1.5 cm^3 .

PACS numbers: 07.55.Ge, 32.80.Bx, 33.35.+r, 76.60.-k

Alkalimetal vapors are used in such vital metrology applications as atomic clocks [1] and magnetometers [2, 3, 4]. In these applications the resolution of frequency measurements of the hyperfine or Zeeman resonance can be improved by increasing the density of alkalimetal atoms until the resonance begins to broaden due to alkalimetal spin-exchange collisions. Such broadening can be completely eliminated for Zeeman resonance near zero magnetic field [5, 6, 7]. The broadening of the hyperfine and Zeeman resonances at a finite magnetic field can be reduced by optically pumping the atoms into a nearly fully polarized state [8, 9, 10]. These techniques have been used to demonstrate clock resonance narrowing [9] and have led to significant improvement in the sensitivity of atomic magnetometers [11] and to their application for detection of magnetic fields from the brain [12] and nuclear quadrupole resonance signals from explosives [13]. However, the effects of spin-exchange collisions on the fundamental sensitivity of atomic clocks and magnetometers operating in a finite magnetic field have not been analyzed.

Here we study theoretically and experimentally the effects of spin-exchange collisions in an atomic magnetometer operating in geomagnetic field range. It was shown in [8, 9, 10] that in the limit of weak excitation the Zeeman and hyperfine resonance linewidths can be reduced from

R_{se} , where R_{se} is the alkalimetal spin-exchange rate, to $(R_{se}R_{sd})^{1/2}$, where R_{sd} is the alkalimetal spin-destruction rate, by pumping most of the atoms into the stretched spin state with maximum angular momentum. Since for alkalimetal atoms $R_{sd} \ll R_{se}$ (for example, for K atoms $R_{sd} \approx 10^4 R_{se}$), this technique can reduce the resonance linewidth by a factor of 10–100. However, the frequency measurement sensitivity depends not only on the linewidth but also on the amplitude of the spin precession signal, and the optimal sensitivity is obtained for an excitation amplitude that leads to appreciable rf broadening. We study the effects of rf broadening in the presence of non-linear evolution due to spin-exchange collisions and find that the fundamental limit on sensitivity is determined by R_{se} even when most atoms are pumped into the stretched spin state and the resonance linewidth is much narrower than R_{se} . We derive a simple

relationship for the ultimate sensitivity of a scalar alkalimetal magnetometer, which also applies qualitatively to atomic clocks.

Scalar magnetometers, which measure the Zeeman resonance frequency proportional to the absolute value of the magnetic field, are important in a number of practical applications, such as mineral exploration [14], searches for archaeological artifacts [15] and unexploded ordnance [16], as well as in fundamental physics experiments, such as searches for a CP-violating electric dipole moment [2]. These applications require magnetometers that can measure small (fT) changes in geomagnetic-size fields with a fractional sensitivity of $10^{-10} \text{--} 10^{-11}$. Existing sensitive scalar magnetometers use large cells filled only with alkalimetal vapor and rely on a surface coating to reduce relaxation of atoms on the walls [2, 3, 4]. However, such coatings generally cannot be used at high temperature necessary to obtain high alkalimetal density. We use helium buffer gas to reduce diffusion of alkalimetal atoms to the walls, which also allows independent measurements of the magnetic field at several locations in the same cell [11]. We present direct measurements of the magnetic field sensitivity in a gradiometric configuration and demonstrate noise level below $10 \text{ fT Hz}^{-1/2}$ in a 10^{-5} T static field (1 part in 10^9) using an active measurement volume $V = 1.5 \text{ cm}^3$. A small active volume and absence of delicate surface coatings opens the possibility of miniaturization and batch fabrication [18] of ultra-sensitive magnetometers. The best previously reported direct sensitivity measurement for a scalar magnetometer, using a comparison of two isotopes of Rb occupying the same volume $V = 180 \text{ cm}^3$, had a standard deviation corresponding to sensitivity of $60 \text{ fT Hz}^{-1/2}$ and fractional sensitivity of $5 \times 10^{-8} \text{ Hz}^{-1/2}$ [17]. Indirect estimates of scalar magnetometer sensitivity on the order of $1 \text{ fT Hz}^{-1/2}$ have been reported in cells with $V = 1000 \text{ cm}^3$ [3, 4].

We rely on a simple magnetometer arrangement using optical pumping with circularly-polarized light parallel to the static magnetic field B_z , excitation of spin coherence with an oscillating transverse magnetic field B_1 , and detection of spin coherence with a probe beam orthogonal to the static field. RF broadening of magnetic resonance is usually described by Bloch equations with phenomeno-

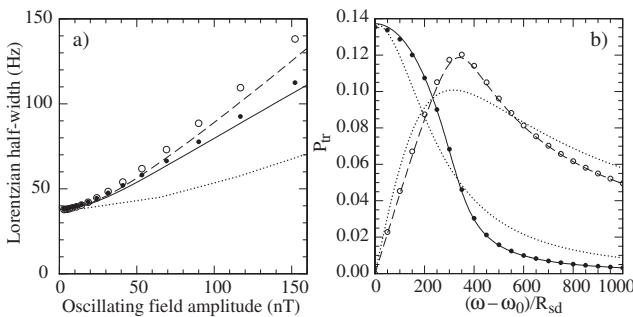


FIG. 1: Panel a: The linewidths of Lorentzian fits to the experimental data for absorption (solid points) and dispersion (open points) components of the magnetic resonance in K vapor at 140 C. The dotted line is the prediction for rf broadening of the linewidth from Bloch equations with constant T_1 and T_2 , the solid and dashed lines are results of Lorentzian fits to absorption and dispersion lineshapes obtained using modified Bloch equations with variable T_2 . In the theory plots, $R_{se} = 5100 \text{ s}^{-1}$ and $R_{sd} = 24 \text{ s}^{-1}$ are fixed from independent measurements, while $R_{op} = 840 \text{ s}^{-1}$ is adjusted to match the linewidth at low rf amplitude. Panel b: Comparison of transverse polarization resonance lineshapes using full numerical density matrix evolution (solid points { absorption, open points { dispersion}) and modified Bloch equations (solid line { absorption, dashed line { dispersion}) for $R_{se}=R_{sd} = 10^4$, $R_{op}=R_{sd} = 200$, $B_1=R_{sd} = 100$. Lorentzian lineshapes are shown with dotted lines for comparison.

logical relaxation times T_1 and T_2 [19]. It was shown in [20] that such a description works for alkali metal atoms in the presence of spin-exchange collisions for small spin polarization. However, the general case of large polarization and large rf broadening, which gives the optimal measurement sensitivity, cannot be described by simple Bloch equations. To study these effects in more detail we performed extensive measurements of magnetic field resonance lineshapes in K vapor for a large range of spin-exchange rates, optical pumping rates, and rf excitation amplitudes. One result of these measurements is shown in Fig. 1a, where we plot the linewidth of a Lorentzian fit to the absorption and dispersion components of the magnetic resonance as a function of the rf excitation amplitude, which is in clear disagreement with simple Bloch equations (dotted line).

More complete results of our experimental measurements and numerical density matrix simulations will be presented elsewhere [21]. Here we derive an analytical result that gives an accurate description of magnetometer behavior in the regime $R_{se} \ll R_{op} \ll R_{sd}$, where R_{op} is the optical pumping rate, applicable to high density alkali metal magnetometers. Based on the theory of optical pumping of alkali vapors in the presence of high density buffer gas [22], it can be shown that the transverse spin relaxation time T_2 for small spin coherences in alkali atoms with $I = 3/2$ is given by

$$\frac{1}{T_2} = \frac{R_{op}}{4} + \frac{R_{se}}{5} (1 - P_z); \quad (1)$$

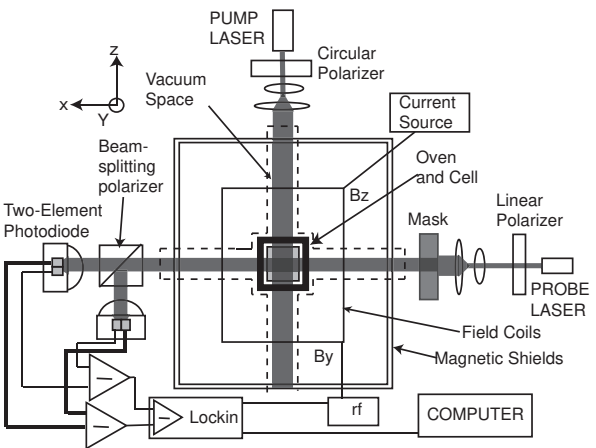


FIG. 2: Schematic of the experimental apparatus. The cell (29 \times 29 \times 40 mm³ with larger dimension perpendicular to lasers) is placed in a glass vacuum enclosure pumped out to 0.5 Torr and heated inside a boron nitride oven. Coils inside 6-layer magnetic shields allow application of magnetic fields and gradients. The gradiometer measurement is obtained by imaging the probe beam onto two-element photodiodes. The signals of the two balanced polarimeters are subtracted at the lock-in that is read through GPIB.

in the regime where the Bloch-Rabi splitting of the magnetic resonance lines is small compared with the spin-exchange rate and the longitudinal spin polarization $P_z = R_{op}/(R_{op} + R_{sd})$ is close to unity [10]. For high P_z most atoms are pumped into $F = 2$ hyperfine manifold and their precession obeys the Bloch equations. Since spin-exchange effects are isotropic, Eq. (1) can be applied for larger excitation with $(1 - P_z)$ replaced by $(1 - P)$, where the vector components of P are given by the Bloch equations [19] with longitudinal spin relaxation time $T_1 = 4 = R_{op}$. Then one obtains an implicit algebraic equation for T_2 that can be solved to calculate P as a function of rf field detuning and other parameters. This model based on modified Bloch equations reproduces the non-Lorentzian resonance lineshape from full density matrix simulation shown in Fig. 1b as well as the experimental rf broadening data shown in Fig. 1a.

The apparatus for sensitive field measurements is shown in Fig. 2. It is built around a Pyrex cell containing potassium in natural abundance, 2.5 atm of ⁴He to slow atomic diffusion, and 60 Torr of N₂ for quenching. The cell is heated to approximately 150 C with pairs of ohmic heaters (wire meander in Kapton sheet) oriented to cancel stray fields and driven at 27 kHz. The K density in the cell is determined from the probe beam absorption spectrum to be $n = 6.4 \times 10^{21} \text{ cm}^{-3}$. A circularly polarized pump beam with a cross-section of roughly 3 \times 1 cm² and power of 20-40 mW tuned to the D 1 transition polarizes the K atoms along the z-direction. The x component of atomic spin polarization is measured using optical rotation of a linearly polarized probe beam with a cross-section of 125 \times 125 cm^2 defined by a mask and power

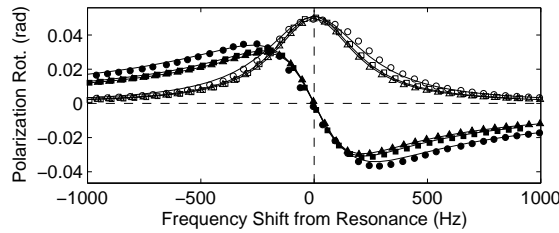


FIG. 3: Absorption (open symbols) and dispersion (closed symbols) components of the magnetic resonance polarization rotation signal at 1 T (squares), 10 T (triangles), and 26 T (circles). Solid lines show best-fit Lorentzians to them measured data.

of 10 mW detuned by about 0.2 nm from the D 1 transition. The optical rotation is measured by two balanced polarimeters using a pair of two-segment photodiodes to form a gradiometer arrangement.

The oscillating rf field B_1 is applied in the y direction with its frequency tuned to the Zeeman resonance given by $\omega_0 = B_z = g_s B_z = (2I+1)^{-1} (700 \text{ kHz}) B_z$ for potassium atoms. The amplitude of the rf field is about 19 nT. Measurements are made for three values of B_z field: 1 T, 10 T, and 26 T.

The polarimeter signals are measured with a lock-in amplifier (Stanford Research Systems SR 830 for 1 and 10 T measurements, SR 844 for the 26 T measurement). The lock-in internal reference is used to generate the rf field, the phase is adjusted to separate the resonance signal into symmetric absorption and antisymmetric dispersion components, and the time constant is set to 100 s. The resonance lineshapes obtained by varying the rf frequency are shown in Fig. 3. The pump power and rf amplitude are adjusted to optimize the slope of the dispersion signal for a given probe beam power. At the parameters that optimize the magnetometer sensitivity, the data are well-described by Lorentzians with similar HWHM for absorption and dispersion components of 215 Hz for 1 and 10 T and 265 Hz for 26 T and amplitudes that are nearly independent of the magnetic field.

The field B_z is generated using custom current sources, based on a mercury battery voltage reference and a FET input stage followed by a conventional op-amp or a transistor output stage [23]. The fractional current noise is less than 2×10^{-8} at 10 Hz, about 10 times better than from a Thorlabs LD C 201 ULN current source. Low-frequency (< 10 Hz) optical rotation noise is reduced by an order of magnitude by covering the optics with boxes to reduce air circulation. The oven and laser beam within the magnetic shields are enclosed in a glass vacuum chamber to reduce convection. Probe beam focusing is adjusted to equalize the photodiode signals for two polarimeters within 2%. The gradiometer measurements reduce by more than an order of magnitude the noise from the B_z current source as well as pump intensity and lightshift noise. By applying a calibrated magnetic field gradient we find the distance between the gradiometer

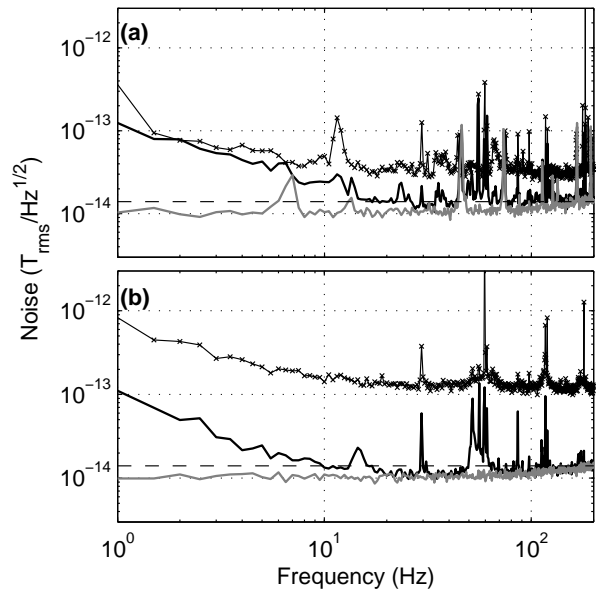


FIG. 4: Noise spectra for 10 mG (a) and 100 mG (b). Shown are single channel spectra (black line with crosses), gradiometer spectra (black solid line), and the measured electronic and optical noise (gray solid line) obtained by blocking the pump beam. The dashed black line marks the $14 \text{ ft}^2/\text{Hz}^{1/2}$ level. Magnetic field noise increases at higher frequencies due to correction for the finite bandwidth of the magnetometer.

channels to be 3.5 mm, much larger than the K discussion length in one relaxation time $(T_2)^{1/2} = 0.1 \text{ mm}$, so the two measurements are independent.

The magnetic field data are acquired from the dispersive lock-in signal for 100 sec with a sampling rate of 2 kHz. The FFT of the data is converted to a magnetic noise spectrum using a frequency calibration of the dispersion slope and corrected for finite bandwidth of the magnetometer. The bandwidth is found to be equal to the Lorentzian HWHM for all values of B_z . The magnetic noise spectra at 1 and 10 T are shown in Fig. 4. At 1 T, single channel measurements are limited by lock-in phase noise, while at 10 T they are limited by current source noise. The gradiometer noise is limited almost entirely by photon shot noise at higher frequencies and reaches below $14 \text{ ft}^2/\text{Hz}^{1/2}$, corresponding to less than $10 \text{ ft}^2/\text{Hz}^{1/2}$ for individual magnetometer channels. With the pump beam blocked, the optical rotation noise is at the photon shot noise level. Low frequency noise is most likely due to remaining effects of convection. At 26 T, the gradiometer has a sensitivity of $29 \text{ ft}^2/\text{Hz}^{1/2}$, limited by imperfect balance between channels and lock-in noise.

The calculation of the fundamental sensitivity for a scalar magnetometer follows closely that for an rf atom interferometer, derived in [10]. The magnetic field spectral noise density is given by

$$B = \frac{\frac{dp}{dt}}{nV} \frac{1}{T_2 + \frac{T_2^2 R_{\text{prOD}}}{16}} + \frac{2}{R_{\text{prOD}}}: \quad (2)$$

where the three terms under the square root correspond to the spin projection noise, light-shift noise from the probe beam, and the photon shot noise. Here V is the active measurement volume, defined by the intersection of the pump and probe beams, $OD = \sigma_0 l$ is the optical depth corresponding to probe propagation distance l , and σ_0 is the light absorption cross-section on resonance. R_{pr} is the probe pumping rate at the actual detuning from the resonance, which contributes to the total spin destruction rate R_{sd} . $dP = d!$ is the slope of the dispersion component of the transverse polarization resonance and

is the efficiency of the photo-detector. The maximum slope of the resonance $dP = d!$ is calculated by optimizing R_{op} and B_1 for a given R_{se} and R_{sd} using the modified Bloch equations with variable T_2 . For $R_{se} = R_{sd}$ we obtain $dP = d! = kR_{se}^{3/4} R_{sd}^{1/4}$ where $k = 12$, in excellent agreement with numerical density matrix calculation.

The optical depth OD on resonance can be optimized by changing the aspect ratio of the cell and the pressure of the buffer gas, which affects σ_0 . For optimal sensitivity $OD = 4^{3/4} 2^{1/2} = (T_2 R_{pr})$ and R_{pr} should be less than R_{sd} due to alkali spin destruction collisions, which generally requires a large OD . In our cell, operating at a relatively low temperature of 150 C with high buffer gas pressure, $OD = 2.5$ and the last term in Eq. (2) dominates, requiring a large R_{pr} . For experimental parameters corresponding to data in Fig. 4 ($R_{se} = 8700 \text{ s}^{-1}$, $R_{pr} = 100 \text{ s}^{-1}$, $R_{sd} = 130 \text{ s}^{-1}$, $V = 1.5 \text{ cm}^3$, and $\eta = 0.24$ including losses in collection of probe light after the cell) we expect magnetic field sensitivity of $3.4 \text{ ft/H z}^{1/2}$ from the Bloch model or $4.5 \text{ ft/H z}^{1/2}$ using the results of the density matrix simulation, which is more accurate because $R_{se} = R_{op} = R_{sd}$ is not fully satisfied. The measured optical shot noise of the magnetometer corresponds to $7 \text{ ft/H z}^{1/2}$ per channel.

Considering a more optimized case when R_{sd} is dominated by K-K spin-destruction collisions, $R_{pr} = R_{sd}$,

and B_1 , R_{op} , and OD are optimized, we find that optimal $T_2 = 1.3 (R_{se} R_{sd})^{1/2}$ and with $R_{se} = nv_{se}$, $B_{min} = 0.94 (v_{se} V)^{1/2} ((1 + (2)^{1/2}))^{1/2}$, where v is the thermal velocity. Using the spin-exchange cross-section $\sigma_{se} = 2 \times 10^{14} \text{ cm}^2$ and $V = 0.5$ we get an optimal magnetic field sensitivity of $1.1 \text{ ft/H z}^{1/2}$ for a 1 cm^3 active volume.

It is interesting to compare the scaling of the optimal magnetic field sensitivities in various regimes. It was shown in [11] that near zero field in spin-exchange relaxation free (SERF) regime the sensitivity scales as $1/2$, while for an rf magnetometer operating in a finite field it scales as $(R_{se} R_{sd})^{1/4}$ [10]. In contrast, here we find that fundamental sensitivity for a scalar magnetometer in a finite field scales as $1/2$, i.e. there is no significant reduction of spin-exchange broadening for optimal conditions. Since σ_{se} is similar for all alkalis, one can expect a similar sensitivity for a Cs or Rb magnetometer. On the other hand, if one is limited by the photon shot noise or technical sources of noise, which is often the case in practical systems, the magnetometer sensitivity is improved because the slope of the dispersion resonance scales as $\sigma_{se}^{3/4} R_{sd}^{1/4}$, instead of $1/\sigma_{se}$. We expect similar relationships, with different numerical factors, to hold for atomic clocks operating on the end transitions, since T_2 in that case is given by an equation similar to Eq. (1) [9].

In conclusion, we have systematically studied spin-exchange effects in a scalar alkali magnetometer. We considered the effects of rf broadening and showed that the best sensitivity for an alkali magnetometer with a 1 cm^3 measurement volume is on the order of $1 \text{ ft/H z}^{1/2}$. We also demonstrated experimentally magnetic field sensitivity below 10 ft/H z with an active volume of only 1.5 cm^3 , opening the possibility for further miniaturization of alkali magnetometers. This work was supported by an ONR MURI grant.

[1] S. Knappe, *Appl. Phys. Lett.* **85**, 1460 (2004).
 [2] S. G roeger, A. S. Pazgalev, and A. W eis, *Appl. Phys. B.* **80**, 645 (2005).
 [3] E. B. A leksandrov et al., *Opt. and Spectr.* **78**, 292 (1995).
 [4] D. Budker, D. F. K imball, S. M. R ochester, V. V. Yashchuk, and M. Zolotorev *Phys. Rev. A* **62**, 043403 (2000).
 [5] W. H apper and H. T ang, *Phys. Rev. Lett.* **31**, 273 (1973).
 [6] W. H apper and A. C. T am, *Phys. Rev. A* **16**, 1877 (1977).
 [7] J. C. A llred, R. N. L yman, T. W. K omack, and M. V. R omalis *Phys. Rev. Lett.* **89**, 130801 (2002).
 [8] S. A ppelt, A. Ben-Amar Baranga, A. R. Young, and W. H apper, *Phys. Rev. A* **59**, 2078 (1999).
 [9] Y.-Y. Jau, et al., *Phys. Rev. Lett.* **92**, 110801 (2004).
 [10] I. M. Savukov, S. J. Seltzer, M. V. R omalis, and K. L. Sauer, *Phys. Rev. Lett.* **95**, 063004 (2005).
 [11] I. K. K omnis, T. W. K omack, J. C. A llred and M. V. R omalis, *Nature* **422**, 596 (2003).
 [12] H. X ia, A. Ben-Amar Baranga, D. H oman, M. V. R omalis, *Appl. Phys. Lett.* (in press).
 [13] S.-K. Lee, K. L. Sauer, S. J. Seltzer, O. A leem, M. V. R omalis, *Appl. Phys. Lett.* (in press).
 [14] M. N. N abighian et al., *Geophys.* **70** 33 (2005).
 [15] A. D avid et al., *Antiquity* **78**, 341 (2004).
 [16] H. H. N elson and J. R. M cDonald, *IEEE Trans. Geosci. Remote Sens.* **39**, 1139 (2001).
 [17] E. B. A leksandrov, M. V. B alabas, A. K. V ershovski, and A. S. Pazgalev, *Tech. Phys.* **49**, 779 (2004).
 [18] P. D. Schw indt et al., *Appl. Phys. Lett.* **85**, 6409 (2004).
 [19] A. A bragam, *Principles of Nuclear Magnetism*, (Oxford University Press, Oxford, 1961).
 [20] N. D. B haskar, J. C amparo, W. H apper, and A. Sham a, *Phys. Rev. A* **23**, 3048 (1981).
 [21] I. M. Savukov, G. Vasilakis, S. J. Sm ullin, and M. V. R omalis, in progress.
 [22] S. A ppelt, et al., *Phys. Rev. A* **58**, 1412 (1998).
 [23] L. Baracchino, G. Basso, C. Cio, and B. N eri, *IEEE Trans. Instrum. Meas.* **46**, 1256 (1997).